Eur. Phys. J. D **13**, 345–353 (2001)

THE EUROPEAN PHYSICAL JOURNAL D

EDP Sciences

Theoretical study of the $A^3 0^+ \leftarrow X^1 0^+$ and $B^3 1 \leftarrow X^1 0^+$ transitions in the Cd-rare gas van der Waals molecules

E. Czuchaj[a], M. Krośnicki, and J. Czub

Institute of Theoretical Physics and Astrophysics, University of Gdańsk, ul. Wita Stwosza 57, 80-952 Gdańsk, Poland

Received 10 August 2000 and Received in final form 7 November 2000

Abstract. Excitation spectra arising from $A^3 0^+ \leftarrow X^1 0^+$ and $B^3 1 \leftarrow X^1 0^+$ electronic transitions in the Cd-rare gas (RG) van der Waals molecules are calculated using newly obtained theoretical potential curves for these species. In the molecular structure calculations, Cd^{20+} and RG^{8+} cores are simulated by energy-consistent pseudopotentials which also account for scalar-relativistic effects and spin-orbit (SO) interaction within the valence shell. Potential energies in the ΛS coupling scheme have been obtained by means of *ab initio* complete-active-space multiconfiguration self consistent-field (CASSCF)/complete-active-space multireference second-order perturbation theory (CASPT2) calculations with a total 28 correlated electrons, while the SO matrix has been computed in a reduced CI space restricted to the CASSCF level. The final Ω potential curves are obtained by diagonalization of the modified SO matrix (its diagonal elements before diagonalization substituted for the corresponding CASPT2 eigen-energies). The spectroscopic parameters for the ground and several excited states of the Cd–RG complexes deduced from the calculated potential curves are in quite reasonable agreement with available experimental data. In addition, the radial Schrödinger equation for nuclear motion was solved numerically with the calculated potentials to evaluate the corresponding vibrational levels and radial wavefunctions. The latter have been used in the calculation of the appropriate Franck-Condon factors to yield information on relative intensities of the vibrational bands of the Cd–RG complexes. The theoretical vibrational progressions are discussed in the context of experimental spectra.

PACS. 33.20.Tp Vibrational analysis – 34.20.-b Interatomic and intermolecular potentials and forces, potential energy surfaces for collisions

1 Introduction

Weakly bound complexes of atoms and small molecules have become the subject of numerous spectroscopic studies in recent years. A great deal of spectroscopic and dynamical information has been accumulated on the van der Waals molecules formed of group IIb metal (M) and rare gas (RG) atoms in the ground and excited states of the former. Detailed information on these species deduced from experimental measurements provides a better understanding of van der Waals bonding as well as interatomic potentials. The latter are important for interpretation of various dynamical processes such as collisional redistribution of resonance radiation, collision-induced singlet-to-triplet energy transfer, electronic orbital alignment, or chemical reactions. Most spectroscopic studies on the M–RG complexes were carried out using supersonic expansion of the metal–RG mixtures from high pressure into vacuum [1–10]. This experimental method serves both as a way of formation and cooling of the van der Waals molecules and permits the study of isolated diatomic complexes through laser excitation and subsequent detection of fluorescence. The fluorescence excitation spectra obtained in this manner are further analyzed by means of the Birge-Sponer (B-S) method which uses a Morse function as representative for each of the potentials involved in an electronic-vibrational transition. It is known, however, that vibrational levels near the dissociation limit often deviate from the linearity of the vibrational spacing $\Delta G_{v+1/2}$ *versus* v, indicating that the Morse potential is not adequate for the long-range part of the potential curve. In such cases the Morse function is combined with a proper term describing the long-range forces between the two atoms to improve an analytical representation of the potential energy curve. This also means that the Birge-Sponer procedure works satisfactorily only near the bottom of the potential well.

Majority of spectroscopic studies on the group IIb–RG complexes are devoted to the Cd–RG and Hg–RG complexes, and concern the molecular states correlating asymptotically with the ground state and the lowest lying $^3P_1$ and $^1P_1$ excited states of the metal atom. Such studies usually provide the spectroscopic characteristics of the potential curves involved in the electronic transition. On the other hand, experimentally determined spectroscopic

[a] e-mail: czu@iftia.univ.gda.pl

constants (D_e, R_e, ω_e) permit a straightforward verification of theoretical interatomic potentials which are still insufficiently known, in spite of substantial progress in both theory and experiment. To our knowledge, so far only three advanced quantum-mechanical calculations on the interaction potentials for the group IIb–RG complexes have been published. In the first study devoted to the Cd-heavy RG atom (Ar, Kr, Xe) species, l-independent statistical pseudopotentials were used to simulate both the Cd-core and RG atoms [11]. For Cd and Hg interacting with light RG atoms (He, Ne), the molecular calculations were performed with more accurate l-dependent pseudopotentials at the valence SCF/CI level [12]. Unfortunately, the obtained theoretical potentials for the Cd–RG and Hg–RG complexes differed appreciably from available experimental data. This discrepancy was roughly interpreted as due to a simplified treatment of the RG atoms in those calculations. Certainly, taking into account the valence electrons of the RG atoms in the molecular calculations explicitly, could improve the description of the metal-RG Pauli repulsion and better account for polarization effects of the RG atoms on the metal atom. However, such advanced many-electron calculations have become feasible only recently after substantial improvements in the applied software (MOLPRO) [13]. In our earlier work on the Cd–RG species [14], the Cd and RG atoms were considered as two- and eight-valence electron systems, respectively, whereas the Cd^{2+} and RG^{8+} cores were represented by scalar-relativistic energy-consistent pseudopotentials. In addition, a core-polarization potential was added to the large-core pseudopotential for Cd to account for core-valence correlation contributions. The computed potential curves were split into Ω components in a semi-empirical manner following the "atoms-in-molecules" model. Comparison of the derived spectroscopic parameters with their experimental values indicated, in general, reasonably good agreement of theory with experiment.

Recently, we have undertaken new molecular calculations on the group IIb–RG complexes, with the aim of removing the still existing deficiencies of the theory. In contrast to our previous calculations on the Cd–RG pairs [14], the metal atom in the present approach is treated as a 20-valence electron system. On the other hand, the M^{20+} and RG^{8+} cores are substituted for *ab initio* scalar-relativistic energy-consistent pseudopotentials supplemented by the corresponding spin-orbit (SO) operators. A detailed description of the potential energy calculations for the Cd–RG complexes with the complete presentation of the results obtained are given in a separate paper [15]. This paper is devoted to the theoretical study of the $A^3 0^+ \leftarrow X^1 0^+$ and $B^3 1 \leftarrow X^1 0^+$ vibrational bands of the Cd–RG van der Waals molecules obtained exclusively on the basis of the calculated potential curves. This also means that the present results are entirely free from fitting to any experimental data. The calculated vibrational bands are also discussed in the context of experimental spectra. After a short presentation of the theory and technical details of the calculations given in Section 3, the results obtained will be discussed in Section 2.

2 Method

2.1 General formulation

The calculation of the adiabatic energies $E_i(R)$ between a group IIb atom (A) and a RG atom (B) in the Born-Oppenheimer approximation reduces to the solution of the Schrödinger equation

$$(H_A + H_B + V_{AB})\Psi_i(\mathbf{x}, \mathbf{R}) = E_i(R)\Psi_i(\mathbf{x}, \mathbf{R}), \quad (1)$$

where H_A and H_B are the Hamiltonians of the isolated atoms A and B, V_{AB} stands for the interaction between the two atoms, $\mathbf{x}$ represents the electronic coordinates, while $\mathbf{R}$ is the position vector of B relative to A. In the present approach the $nsnpnd$ core electrons and $(n+1)$ $s(n=4)$ valence electrons of the atom A are considered on an equal footing. Consequently, the twenty valence electrons of the atom A and eight valence electrons of the atom B are treated explicitly, while the A^{20+} and B^{8+} cores as well as valence-shell scalar-relativistic effects and SO interaction are represented by lj-dependent quasirelativistic pseudopotentials. The valence model Hamiltonian in (1) can be written (in atomic units) as

$$H = -\frac{1}{2}\sum_i \Delta_i + V_{\mathrm{av}} + V_{\mathrm{so}} + \sum_{j>i=1}^{N} \frac{1}{r_{ij}} + \sum_{\lambda>\mu} \frac{Q_\lambda Q_\mu}{r_{\lambda\mu}}, \quad (2)$$

where i, j denote valence electrons, λ, μ are core indices and Q_λ, Q_μ represent core charges. The SO averaged pseudopotential V_{av}, which accounts for scalar-relativistic effects, has the following semilocal form

$$V_{\mathrm{av}} = -\sum_{\lambda,i} \frac{Q_\lambda}{r_{\lambda i}} + \sum_{\lambda,i}\sum_{l,k} A_{\lambda lk} \exp(-a_{\lambda lk} r_{\lambda i}^2) P_{\lambda l}, \quad (3)$$

where $P_{\lambda l}$ is the projection operator onto the Hilbert subspace of angular symmetry l with respect to core λ

$$P_{\lambda l} = \sum_{m=-l}^{l} |\lambda l m\rangle\langle\lambda l m|. \quad (4)$$

In turn the pseudopotential representing the SO operator takes the form

$$V_{\mathrm{so}} = \sum_{\lambda,i}\sum_{l} \frac{2\Delta V_{i,\lambda l}}{2l+1} P_{\lambda l} \mathbf{l}_i \mathbf{s}_i P_{\lambda l}. \quad (5)$$

The difference $\Delta V_{i,\lambda l}$ of the radial parts of the two-component quasirelativistic pseudopotentials $V_{\lambda l, l+1/2}$ and $V_{\lambda l, l-1/2}$ is expressed in terms of Gaussian functions

$$\Delta V_{i,\lambda l} = \sum_k \Delta A_{\lambda lk} \exp(-a_{\lambda lk} r_{\lambda i}^2). \quad (6)$$

In the case of small-core pseudopotentials the polarization potential which describes, among others, core-valence correlation effects is usually disregarded, because the dipole polarizabilities of the cores are small. The last term in equation (2) represents the core-core interaction. Since the A^{20+} and B^{8+} cores are well separated, we choose a simple point-charge Coulomb interaction in this case.

2.2 Details of calculations

High-level valence *ab initio* calculations have been carried out for the ground and several excited states of the Cd–RG species. The cadmium and RG atoms in the present approach are treated as 20- and 8-valence electron species, respectively. The free parameters occurring in $V_{\rm av}$ and $V_{\rm so}$, defined by equations (3, 5, 6), for the Cd atom were taken from [16]. The corresponding optimized primitive $(8s7p6d)$ basis set taken from [16] has been augmented with one diffuse *s*-, *p*- and *d*-function. A polarization set of four *f*-functions and two *g*-functions taken from [17] was also added. The final contracted basis set for Cd used in the calculations is designated as $(9s8p7d4f2g)/[8s7p6d4f2g]$. In turn the one-component relativistic energy-consistent *ab initio* pseudopotentials for the RG atoms, supplemented with effective spin-orbit potentials, were taken from Nicklass *et al.* [18]. For He we used the contracted $(13s8p5d3f)/[7s8p5d3f]$ basis set with *s*-functions taken from [19], *p*- and *d*-functions derived from [20] and *f*-functions taken from the augmented correlation-consistent polarized valence-quintuple-zeta (aug-cc-pV5Z) basis set [21]. For Ne, Ar, Kr and Xe we started with the optimized uncontracted basis sets taken from Nicklass *et al.* [18] ($7s7p3d$ for Ne, $6s6p3d$ otherwise). These basis sets were augmented with diffuse *s*-, *p*- and *d*-functions determined by means of even-tempered continuation of the series of low exponents of the corresponding Nicklass'es basis. In addition, three *f*-functions were added in each case to improve description of the polarization of the RG atoms. Finally, we used an uncontracted $(9s9p4d3f)$ basis set for Ne and a contracted $[8s7p4d3f]$ one for the remaining RG atoms.

The potential energy curves have first been evaluated in the ΛS coupling scheme by means of complete-active-space multiconfiguration self-consistent-field (CASSCF) calculations followed by complete-active-space multireference second-order perturbation theory (CASPT2) calculations with an open-shell correction term to the one-electron Fock operator as proposed by Werner [22]. The active space is spanned by the molecular counterparts of the valence $5s5p$ and Rydberg $6s6p$ orbitals of Cd in the C_{2v} point group. The molecular orbitals used in the calculations were determined in a *state-averaged* CASSCF with the same weight for the ground and excited states. The valence orbitals of the RG atom and the $4s4p4d$ orbitals of Cd were kept doubly occupied in all configuration-state functions (CSFs). However, they were fully optimized in the CASSCF calculations and correlated through single and double excitations from the reference configurations in the CASPT2 calculations. The next step involves the inclusion of spin-orbit coupling at the CI level. In the present approach the SO matrix elements are computed using the SO pseudopotentials for both the Cd and RG atoms. The SO eigenstates are obtained by diagonalization of the $H_{\rm el} + H_{\rm so}$ matrix in a basis formed of selected spatial configurations multiplied by appropriate spin functions. The resulting products are grouped together according to symmetry to form an appropriate matrix for each of the four C_{2v} double group representations. In the present calculations the off-diagonal elements of the SO operator are computed employing the truncated version of the CI space restricted to the CASSCF wavefunctions. However, to account for correlation effects at a higher level of theory, the diagonal elements of the SO matrix before diagonalization were replaced by the precomputed CASPT2 eigen-energies. It has been found that the basis-set superposition error (BSSE) is appreciable in the present calculations and has to be taken into account if the calculated potential curves are to be used in a detailed analysis of the Cd–RG vibrational spectra. BSSE has been eliminated using the standard counterpoise method [23]. The calculations of the potential curves have been carried out using the MOLPRO program code by Werner and Knowles [13]. More information on details of the molecular structure calculations is given in [15].

In order to calculate the vibrational progressions for the Hg–RG complexes, the radial Schrödinger equation for nuclear motion was solved numerically by means of the Numerov-Cooley method using the appropriate potential curve for each case. By counting the number of nodes of the wavefunction resulting from the integration of the Schrödinger equation we were able unambiguously to assign a quantum number v to the calculated eigenvalue of energy. The wavefunctions have been subsequently used in the calculations of appropriate Franck-Condon (F-C) factors defining relative intensities of the vibrational bands.

3 Results and discussion

In this paper we discuss only the relevant potential curves of the Cd–RG species correlating with the $(5s^2)^1$S ground and $(5s5p)^3P_1$ excited states of the Cd atom. Due to a large energy gap (31 246 cm^{-1}) between the triplet state and the ground state of Cd, the influence of the SO interaction on the latter proves to be unimportant. However, the SO interaction becomes essential for the Ω-states correlating to different fine-structure components of the Cd $(5s5p)^3P_j$ triplet state. Two molecular states correlate asymptotically to the Cd $^3P_1$ state. One of them labeled $A^3 0^+$ is a nearly pure $^3\Pi$ state as a result of weak interaction with the state of the same symmetry correlating to the Cd $(5s5p)^1P_1$ atomic state. The second state labeled $B^3 1$ is of mixed $\Sigma{-}\Pi$ character due to SO coupling. In consequence, the $A^3 0^+$ potential curve is much deeper than the ground $X^1 0^+$ state, while exactly the reverse is true for the $B^3 1$ state. Typically, two groups of vibrational bands in the excitation spectra appear in the red and blue regions of the intercombination line of the group IIb metal-atom interacting with a RG atom in the ground state. These bands are assigned to electronic transitions from the ground state to the $A^3 0^+$ and the $B^3 1$ molecular states, respectively.

3.1 CdXe

The calculated ground-state potential curve for CdXe is characterized by the potential well depth $D_{\rm e} = 192$ cm^{-1}

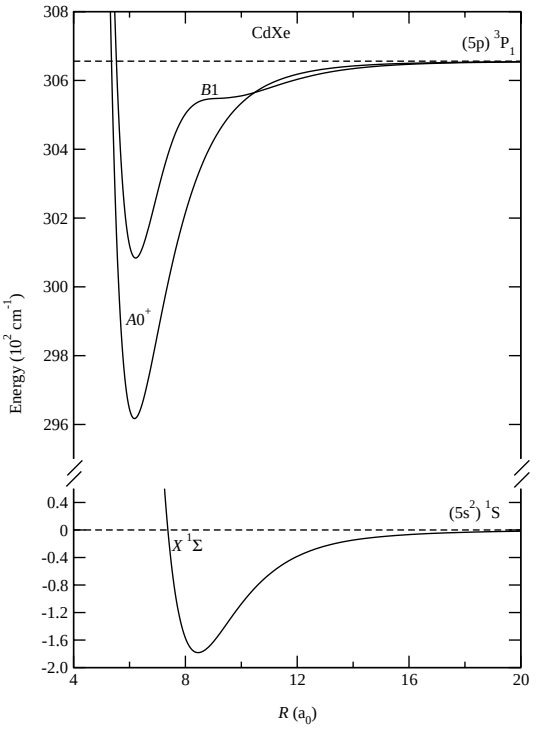

Fig. 1. Potential curves for the ground $X^1\Sigma^+$ and two excited A^30^+ and B^31 states of CdXe.

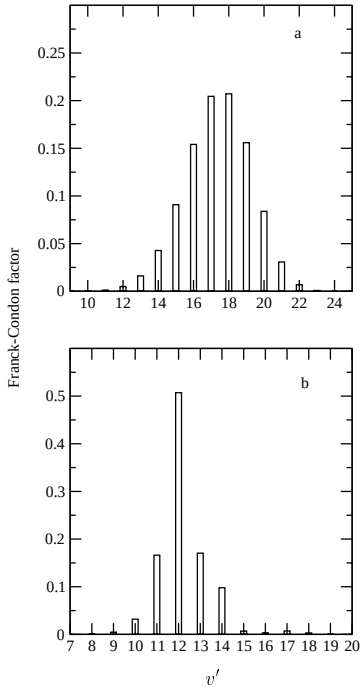

Fig. 2. Calculated Franck-Condon factors for: (a) $A0^+(v') \leftarrow X(v''=0)$, (b) $B1(v') \leftarrow X(v''=0)$ transitions in CdXe.

(192 cm^{-1} [24]) and equilibrium position $R_e = 8.41a_0$ ($8.09a_0$ [24]). Numbers in parentheses here and below denote the experimental values. The A^30^+ potential curve exhibits a relatively deep minimum with $D_e = 1040$ cm^{-1} (1086 ∓ 40 cm^{-1} [4]) at $R_e = 6.18a_0$, and changes regularly with increasing R approaching the dissociation limit at about $R = 20a_0$. Both the potential curves are plotted in Figure 1. Figure 2a presents the Franck-Condon factors (F-C overlap integral squared) calculated for the $A(v') \leftarrow X(v''=0)$ transitions. As seen from the diagram, the substantially larger from zero F-C factors comprise the $v' \leftarrow v''=0$ transitions with v' ranging from 13 to 21 of a total 47 vibrational levels calculated for the A^30^+ state. Comparing this diagram with the $A \leftarrow X$ fluorescence excitation spectrum of CdXe reported by Kvaran *et al.* [4] one finds very good agreement of theory with experiment. One has to stress, however, that our diagram presents only F-C factors and not full band intensities. Note also that the Kvaran's v'-assignment of the bands is given with an uncertainty of $\Delta v' = \pm 1$. On the other hand, the B^31 potential curve of CdXe, deviates appreciably from regularity as seen from Figure 1. This potential curve possesses a minimum at $R_e = 6.22a_0$ with $D_e = 572$ cm^{-1} (152 cm^{-1} [24]). With increase of internuclear separation the potential curve has a shoulder at about $R_e = 8.5a_0$, and next rises slowly towards the dissociation asymptote. The calculated Franck-Condon factors for the $B1 \leftarrow X$ transition are shown in Figure 2b. As seen from the diagram, theory predicts here the $v' \leftarrow v''=0$ transitions with v' ranging merely from 10 to 14 of a total 35 vibrational levels calculated for the B^31 state. Since we are not aware of any excitation spectra measured for the $B1 \leftarrow X$ transition of CdXe, our theoretical prediction cannot be compared with experiment in this case. Large discrepancy between the theoretical potential well depth and its experimental counterpart for the $B1$ state of CdXe can be easily understood. In light of the present calculations, the experimental value of D_e of the $B1$ potential for CdXe is likely in error. According to the classical F-C principle, only selective $A \leftarrow X$ electronic-vibrational transitions in CdXe take place (large $\Delta R_e = R_e'' - R_e'$). This prevents from precise determination of the excited-state potential well depth. The calculated frequencies of the vibrational bands for CdXe are listed in Table 1.

3.2 CdKr

The ground-state potential curve of CdKr has a minimum at $R_e = 8.20a_0$ ($8.18a_0$ [2]) with $D_e = 145$ cm^{-1} (130 cm^{-1} [25]). In turn the A^30^+ potential is characterized by $D_e = 568$ cm^{-1} (529 cm^{-1} [4]) and $R_e = 6.24a_0$ and behaves regularly *versus* R in the entire internuclear separation range. Both the potential curves along with selected vibrational wavefunctions are shown in Figure 3. Figure 4a presents the appropriate Franck-Condon factors. As seen from the figure, the $A(v') \leftarrow X(v''=0)$ transitions in CdKr can take place only for v' ranging at most from 6 to 14. The total number of vibrational levels calculated for the A^30^+ state of CdKr amounts to 33. Comparing the diagram from Figure 4a with the corresponding experimental fluorescence excitation spectrum reported by Kvaran *et al.* [4] one can easily see that the

Table 1. Calculated frequencies of vibrational transitions for CdXe.

	$A\,^3 0^+ \leftarrow X\,^1 0^+$		$B\,^3 1 \leftarrow X\,^1 0^+$	
$v' \leftarrow v''$	$\tilde{\nu}$ (cm^{-1})	ΔG (cm^{-1})	$\tilde{\nu}$ (cm^{-1})	ΔG (cm^{-1})
$10 \leftarrow 0$			30679.6	
				24.0
$11 \leftarrow 0$			30703.6	
				19.0
$12 \leftarrow 0$			30722.5	
				10.6
$13 \leftarrow 0$	30382.6		30733.1	
		32.6		5.6
$14 \leftarrow 0$	30415.2		30738.8	
		31.2		
$15 \leftarrow 0$	30446.4			
		29.9		
$16 \leftarrow 0$	30476.3			
		28.5		
$17 \leftarrow 0$	30504.8			
		27.2		
$18 \leftarrow 0$	30532.0			
		25.9		
$19 \leftarrow 0$	30557.9			
		24.6		
$20 \leftarrow 0$	30582.6			
		23.3		
$21 \leftarrow 0$	30605.9			

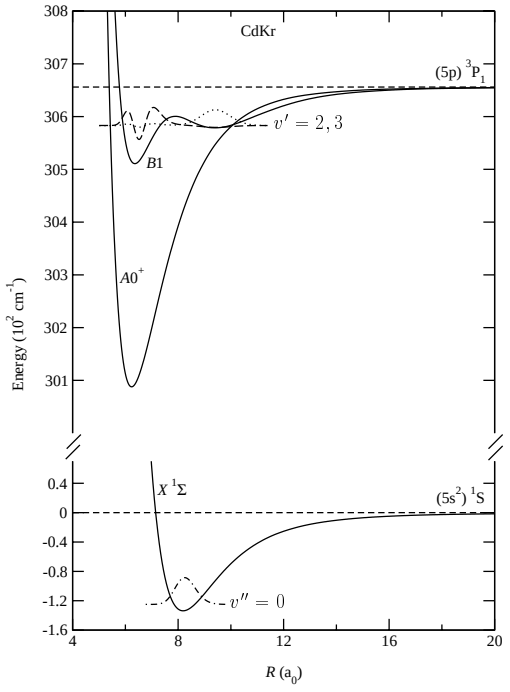

Fig. 3. Potential curves for the ground $X^1\Sigma^+$ and two excited $A^3 0^+$ and $B^3 1$ states of CdKr.

theoretical prediction of this spectrum nearly exactly reproduces its experimental counterpart, provided that the theoretical $v' = 6 \leftarrow v'' = 0$ transition is ascribed to their last detectable $A(v' = 4) \leftarrow X(v'' = 0)$ band lying on the long-wavelength side of the atomic line. As seen, even relative intensities of both the progressions are in excellent agreement. Concerning the results reported by Czajkowski *et al.* [7], it seems that our very weak $v' = 5 \leftarrow v'' = 0$

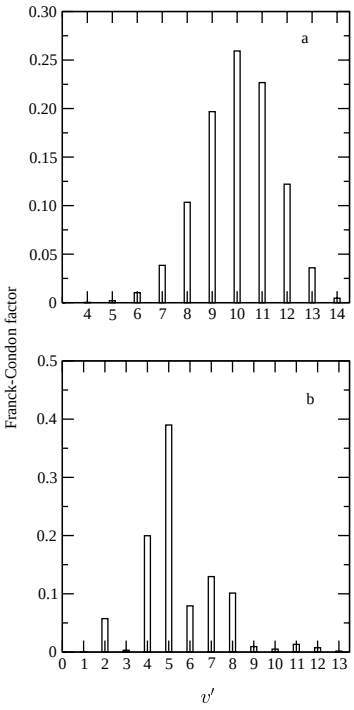

Fig. 4. Calculated Franck-Condon factors for: (a) $A0^+(v') \leftarrow X(v'' = 0)$, (b) $B1(v') \leftarrow X(v'' = 0)$ transitions in CdKr.

band might correspond to their $v' = 3 \leftarrow v'' = 0$ band (*cf.* Fig. 5 in [7]) undetected, however, by the former authors. The $B^3 1$ potential curve for CdKr proves to be of most interest due to its double minimum. The inner potential well being the result of SO interaction has a minimum characterized by $D_e = 145$ cm^{-1} and $R_e = 6.37 a_0$. This minimum is separated from an outer shallow minimum ($D_e = 77$ cm^{-1}, $R_e = 9.38 a_0$), by a potential barrier localized near $R = 8.5 a_0$. Such a shape of the $B^3 1$ potential curve has undoubtedly to affect the $B \leftarrow X$ spectrum. Figure 3 also shows the vibrational wavefunctions of the two ($v' = 2$ and 3) nearly degenerated levels. The present calculations show that the vibrational levels with $v' = 2$ and 3 coincide, but are attributed to different potential wells. According to the Franck-Condon principle, a transition from $v'' = 0$ to $v' = 3$ should not take place since the latter level is associated with the inner potential well (large ΔR_e). Furthermore, the calculated vibrational levels with $v' = 5$ and 6 are separated from each other by only 3.8 cm^{-1}. Due to limited resolution of the detection system they were likely unrecognizable in the trace of the corresponding excitation spectrum reported by Czajkowski *et al.* (*cf.* Fig. 1 in [7]), and were rather seen as one band slightly broadened from the blue side at the bottom. Finally, theory predicts in this case a progression consisting of five vibrational bands covering in fact the v'-range extending from $v' = 2$ to $v' = 8$ of a total 23 vibrational states calculated for the $B^3 1$ state. The strongest $v' \leftarrow v''$ band corresponds to the $v' = 5 \leftarrow v'' = 0$ transition. This prediction agrees entirely with the experimental results of Czajkowski *et al.* [7] except for a slightly different v'-assignment of the bands which is quite understood,

Table 2. Calculated frequencies of vibrational transitions for CdKr.

	$A\,^3\Sigma^+ \leftarrow X\,^1\Sigma^+$		$B\,^3\Pi \leftarrow X\,^1\Sigma^+$	
$v' \leftarrow v''$	$\tilde{\nu}$ (cm^{-1})	ΔG (cm^{-1})	$\tilde{\nu}$ (cm^{-1})	ΔG (cm^{-1})
$2 \leftarrow 0$			30719.0 (30706.1)[a]	
$3 \leftarrow 0$			30719.3	
				8.0 (8.9)
$4 \leftarrow 0$	30395.2 (30388.3)		30727.0 (30715.0)	
		33.5 (33.2)		7.0 (8.5)
$5 \leftarrow 0$	30428.7 (30421.5)		30734.0 (30723.5)	
		31.8 (30.5)		
$6 \leftarrow 0$	30460.6 (30452.0)		30737.8 (30731.6)	
		30.2 (29.1)		7.9 (8.1)
$7 \leftarrow 0$	30490.8 (30481.1)		30742.0 (30739.3)	
		28.6 (28.1)		5.6 (7.7)
$8 \leftarrow 0$	30529.4 (30509.2)		30747.4 (30746.4)	
		27.1 (27.1)		
$9 \leftarrow 0$	30546.5 (30536.3)			
		25.5 (24.7)		
$10 \leftarrow 0$	30572.0 (30561.0)			
		24.0 (23.5)		
$11 \leftarrow 0$	30596.0 (30584.5)			
		22.4 (22.5)		
$12 \leftarrow 0$	30618.4 (30607.0)			
		20.9 (21.0)		
$13 \leftarrow 0$	30639.3 (30628.0)			
		19.4		
$14 \leftarrow 0$	30658.8			

[a]Numbers in parentheses denote experimental values [7].

inasmuch as these authors ascribed the first detectable component of the spectrum on the long-wavelength side of the atomic line to the $v' = 0 \leftarrow v'' = 0$ transition. As can also see from the diagram in Figure 4b, transitions from $v'' = 0$ to higher than $v' = 8$ vibrational levels of the $B^3\Pi$ state of CdKr are very weak and experimentally rather undetectable. The calculated frequencies of the vibrational bands for CdKr are gathered in Table 2.

3.3 CdAr

The calculated ground-state potential curve for CdAr is characterized by the potential well depth $D_e = 107$ cm^{-1} (107 cm^{-1} [4]) and equilibrium position $R_e = 8.11a_0$ ($8.13a_0$ [4]). The $A^3\Sigma^+$ potential curve of CdAr has a minimum at $R_e = 6.37a_0$ with $D_e = 324$ cm^{-1} (325 cm^{-1} [4]) and with increasing internuclear separation regularly approaches the dissociation asymptote. The total number of vibrational energy levels calculated for the $A^3\Sigma^+$ state amounts to 18. Both the potential curves are shown in Figure 5. Figure 6a illustrates the calculated Franck-Condon

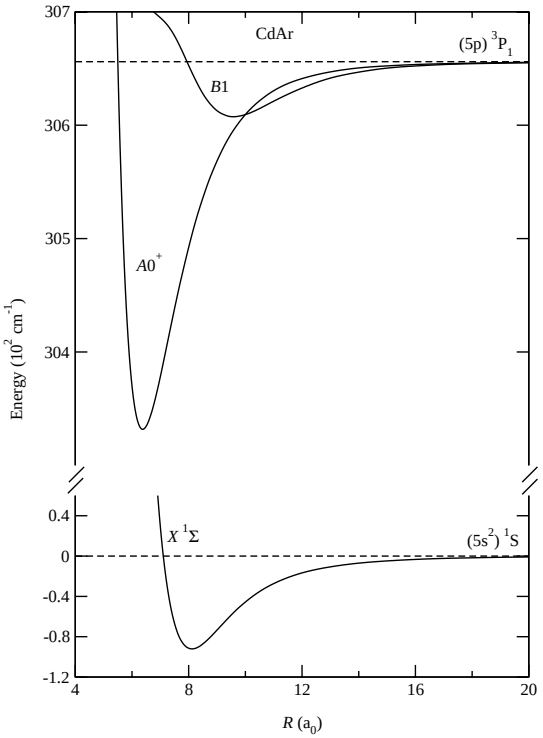

Fig. 5. Potential curves for the ground $X^1\Sigma^+$ and two excited $A^3\Sigma^+$ and $B^3\Pi$ states of CdAr.

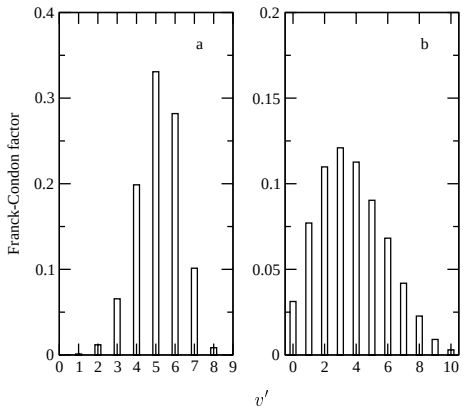

Fig. 6. Calculated Franck-Condon factors for: (a) $A0^+(v') \leftarrow X(v'' = 0)$, (b) $B1(v') \leftarrow X(v'' = 0)$ transitions in CdAr.

factors for the $A^3\Sigma^+ \leftarrow X^1\Sigma^+$ transition in CdAr. As seen, the $v' \leftarrow v'' = 0$ theoretical bands corresponding to v' ranging from 1 to 7 nearly exactly reproduce the experimental results of Kvaran *et al.* [4] and Bobkowski *et al.* [6]. In this case, both theory and experiment unambiguously show that the $A \leftarrow X$ excitation spectrum of CdAr consists of seven vibrational bands, although the $A^3\Sigma^+$ potential well accommodates 18 vibrational levels. The relevant portion of the calculated $B^3\Pi$ potential curve is plotted in Figure 5. The structured short-range part of the potential is not displayed here. The potential curve is characterized by $D_e = 48$ cm^{-1} (56 cm^{-1} [1]) and $R_e = 9.62a_0$ ($9.47a_0$ [1]). The appropriate Franck-Condon factors are shown in Figure 6b. The total number of calculated vibrational

Table 3. Calculated frequencies of vibrational transitions for CdAr.

	$A\,^3 0^+ \leftarrow X\,^1 0^+$		$B\,^3 1 \leftarrow X\,^1 0^+$	
$v' \leftarrow v''$	$\tilde{\nu}$ (cm^{-1})	ΔG (cm^{-1})	$\tilde{\nu}$ (cm^{-1})	ΔG (cm^{-1})
$0 \leftarrow 0$			30709.7 (30707.8)[a]	
				9.1 (10.6)
$1 \leftarrow 0$	30485.8 (30486.7)		30718.8 (30718.4)	
		34.5 (35.3)		8.0 (9.3)
$2 \leftarrow 0$	30520.3 (30522.0)		30726.7 (30727.7)	
		32.0 (31.0)		6.9 (8.4)
$3 \leftarrow 0$	30552.2 (30553.0)		30733.6 (30736.1)	
		29.4 (28.8)		5.9 (7.0)
$4 \leftarrow 0$	30581.6 (30581.8)		30739.5 (30743.0)	
		26.9 (27.0)		4.8 (5.9)
$5 \leftarrow 0$	30608.6 (30608.8)		30744.3 (30748.9)	
		24.5 (25.0)		3.7 (4.9)
$6 \leftarrow 0$	30633.1 (30633.8)		30747.9 (30753.8)	
		22.0 (22.5)		2.6 (3.5)
$7 \leftarrow 0$	30655.0 (30656.3)		30750.6 (30757.3)	
		19.6		1.6 (2.4)
$8 \leftarrow 0$	30674.6		30752.2 (30759.7)	
				0.7 (1.8)
$9 \leftarrow 0$			30752.9 (30761.5)	
				0.3 (0.4)
$10 \leftarrow 0$			30753.2 (30761.9)	

[a]Numbers in parentheses denote experimental values [6].

levels in the $B^3 1$ state amounts to 11. As seen from Figure 6b, the theoretical v'-progression encompasses $v' \leftarrow v'' = 0$ transitions to all the v'-levels generated by the $B^3 1$ potential which agrees entirely with the experimental evidence [6]. The calculated frequencies of the vibrational bands for CdAr are collected in Table 3.

3.4 CdNe

The calculated ground-state potential curve for CdNe has a minimum at $R_e = 7.98 a_0$ ($8.14 a_0$ [26]) with $D_e = 34$ cm^{-1} (28.3 cm^{-1} [26]), but the $A^3 0^+$ potential is characterized by $D_e = 53$ cm^{-1} (70.5 cm^{-1} [26]) and $R_e = 6.83 a_0$. Both the potential curves are shown in Figure 7. Figure 8a illustrates the calculated Franck-Condon factors for the $A^3 0^+ \leftarrow X^1 0^+$ transition in CdNe. The total number of calculated vibrational states in the $A^3 0^+$ state of CdNe amounts to 7. However, both theory and experiment [4–6] show that only three of them participate in formation of the corresponding vibrational spectrum. It turns out that both the theoretical and experimental $v' = 2 \leftarrow v'' = 0$ band lies on the blue side of the Cd (^{3}P$_1 \leftarrow {}^1$S$_0$) atomic line. In turn the calculated $B^3 1$ potential curve for CdNe possesses a minimum

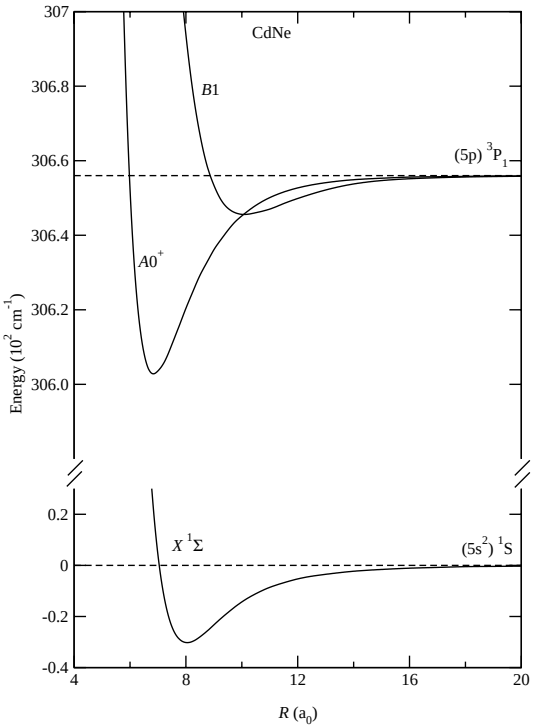

Fig. 7. Potential curves for the ground $X^1\Sigma^+$ and two excited $A^3 0^+$ and $B^3 1$ states of CdNe.

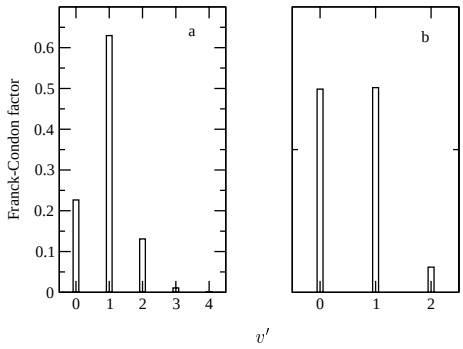

Fig. 8. Calculated Franck-Condon factors for: (a) $A0^+(v') \leftarrow X(v''=0)$, (b) $B1(v') \leftarrow X(v''=0)$ transitions in CdNe.

at $R_e = 10.08 a_0$ with $D_e = 10$ cm^{-1} (9.6 cm^{-1} [26]), as shown in Figure 7. The $B^3 1$ potential accommodates three vibrational levels. Figure 8b illustrates the corresponding Franck-Condon factors. In the case of the $B^3 1$ state, the theoretical prediction disagrees with the experimental results reported in [6] as to the number of $B^3 1 \leftarrow X^1 0^+$ vibrational bands, but is completely confirmed by the very recent measurements [26]. The calculated frequencies of the vibrational bands for CdNe are listed in Table 4.

3.5 CdHe

The CdHe complex represents the weakest van der Waals molecule of the Cd–RG series. To our knowledge, there has appeared so far the only one experimental work devoted to this species [10]. The very shallow potential curves for

Table 4. Calculated frequencies of vibrational transitions for CdNe.

	$A\,^3\Sigma^+ \leftarrow X\,^1\Sigma^+$		$B\,^3\Pi \leftarrow X\,^1\Sigma^+$	
$v' \leftarrow v''$	$\tilde{\nu}$ (cm^{-1})	ΔG (cm^{-1})	$\tilde{\nu}$ (cm^{-1})	ΔG (cm^{-1})
$0 \leftarrow 0$	30638.9		30674.7	
	(30621.3)[a]		(30670.7)	
		16.5 (19.7)		4.5 (4.3)
$1 \leftarrow 0$	30655.4		30679.3	
	(30641.0)		(30675.0)	
		12.2 (17.2)		2.4 (3.3)
$2 \leftarrow 0$	30667.6		30681.7	
	(30658.2)		(30678.3)	

[a]Numbers in parentheses denote experimental values [6].

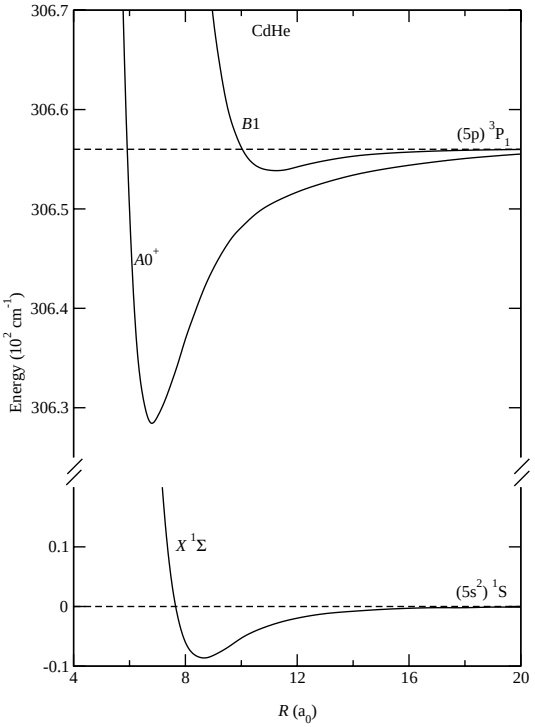

Fig. 9. Potential curves for the ground $X^1\Sigma^+$ and two excited $A^3\mathrm{0}^+$ and $B^3\mathrm{1}$ states of CdHe.

the ground and the lowest lying excited-states of CdHe are presented in Figure 9. In particular, the calculated $X^1\mathrm{0}^+$ potential curve has the dissociation energy $D_\mathrm{e} = 9.0$ cm^{-1} (14.2 cm^{-1} [10]) and equilibrium position $R_\mathrm{e} = 8.25a_0$ ($8.18a_0$ [10]). The $A^3\mathrm{0}^+$ and $B^3\mathrm{1}$ excited-state potentials are characterized by $D_\mathrm{e} = 27.5$ cm^{-1} (41.2 cm^{-1} [10]), $R_\mathrm{e} = 6.75a_0$ ($5.35a_0$ [10]) and $D_\mathrm{e} = 2.2$ cm^{-1} (6.1 cm^{-1} [10]), $R_\mathrm{e} = 11.30a_0$ ($8.41a_0$ [10]), respectively. Both $A^3\mathrm{0}^+ \leftarrow X^1\mathrm{0}^+$ and $B^3\mathrm{1} \leftarrow X^1\mathrm{0}^+$ transitions take place very close to the Cd ($5^3\mathrm{P}_1 \leftarrow 5^1\mathrm{S}_0$) atomic transition. The whole spectrum spreads out over a small range of wavelengths about the atomic line. The present calculations predict that the CdHe ground-state potential supports only one bound vibrational state lying 2.6 cm^{-1} below the dissociation limit. In turn the $A^3\mathrm{0}^+$ potential curve accommodates three bound vibrational levels situated 14.8, 3.2 and 0.2 cm^{-1} below the dissociation asymptote for $v' = 0, 1$ and 2, respectively. Finally, the very shallow $B^3\mathrm{1}$ potential supports merely one vibrational level located 0.2 cm^{-1} below the dissociation limit. The calculated Franck-Condon factors 0.31, 0.66 and 0.01, correspondingly for $v' = 0, 1$ and 2 of the $A(v') \leftarrow X(v'' = 0)$ transitions indicate that one should expect only two vibrational bands on the long-wavelength side of the Cd atomic line. On the other hand, one band on the short-wavelength side of the atomic line is predicted as a result of the $B\mathrm{1}(v' = 0) \leftarrow X(v'' = 0)$ transition for which the evaluated F-C factor amounts to 0.27. Frequencies of the corresponding vibrational transitions from the $X^1\mathrm{0}^+(v'' = 0)$ level to the upper states of CdHe are gathered in Table 5. The theoretical prediction for CdHe differs slightly from the results reported by Koperski and Czajkowski [10]. However, one has to stress that in the case of so weakly bound molecules like CdHe both theory and experiment are often encumbered with a relatively large error.

Table 5. Calculated frequencies of vibrational transitions for CdHe.

	$A\,^3\Sigma^+ \leftarrow X\,^1\Sigma^+$		$B\,^3\Pi \leftarrow X\,^1\Sigma^+$	
$v' \leftarrow v''$	$\tilde{\nu}$ (cm^{-1})	ΔG (cm^{-1})	$\tilde{\nu}$ (cm^{-1})	ΔG (cm^{-1})
$0 \leftarrow 0$	30643.7		30658.4	
	(30633.2)[a]		(30661.9)	
		11.7 (15.4)		
$1 \leftarrow 0$	30655.4			
	(30648.6)			
		2.9 (10.7)		
$2 \leftarrow 0$	30658.3			
	(30659.3)			

[a]Numbers in parentheses denote experimental values [10].

4 Conclusions

Potential energy curves for the Cd–RG van der Waals molecules have been calculated at the valence CASSCF/CASPT2 level including SO coupling. The Cd^{20+} and RG^{8+} cores as well as scalar-relativistic effects and SO interaction were modeled by lj-dependent energy-consistent pseudopotentials. Quite reasonably good agreement of the calculated potentials with available experimental data has been obtained for all the Cd–RG combinations. The calculated vibrational progressions associated with the $A^3\mathrm{0}^+ \leftarrow X^1\mathrm{0}^+$ and $B^3\mathrm{1} \leftarrow X^1\mathrm{0}^+$ electronic transitions for the Cd–RG species have been evaluated exclusively on the basis of the potential curves obtained. The calculations clearly indicate that for majority of the Cd–RG complexes only selective excitations of vibrational levels in the $A^3\mathrm{0}^+$ and $B^3\mathrm{1}$ states take place. The theoretical v'-progressions for all Cd–RG pairs prove to be reasonably consistent with their experimental counterparts. The present results are believed to be helpful in both an identification and a better understanding of the observed $A \leftarrow X$ and $B \leftarrow X$ spectra produced by the Cd–RG van der Waals molecules.

This work was supported by the KBN under grant No. PB1124/P03/97/12. One of us (E.C.) wishes to thank Dr. W. Miklaszewski for his help in numerical calculations.

References

1. A. Kowalski, M. Czajkowski, W.H. Breckenridge, Chem. Phys. Lett. **121**, 217 (1985).
2. D.J. Funk, A. Kvaran, W.H. Breckenridge, J. Chem. Phys. **90**, 2915 (1989).
3. D.J. Funk, W.H. Breckenridge, J. Chem. Phys. **90**, 2927 (1989).
4. A. Kvaran, D.J. Funk, A. Kowalski, W.H. Breckenridge, J. Chem. Phys. **89**, 6069 (1989).
5. R. Bennett, W.H. Breckenridge, J. Chem. Phys. **96**, 882 (1992).
6. R. Bobkowski, M. Czajkowski, L. Krause, Phys. Rev. A **41**, 243 (1990).
7. M. Czajkowski, R. Bobkowski, L. Krause, Phys. Rev. A **44**, 5730 (1991).
8. M. Czajkowski, R. Bobkowski, L. Krause, Phys. Rev. A **45**, 6451 (1992).
9. M. Czajkowski, L. Krause, R. Bobkowski, Phys. Rev. A **49**, 775 (1994).
10. J. Koperski, M. Czajkowski, J. Chem. Phys. **109**, 459 (1998).
11. E. Czuchaj, J. Sienkiewicz, J. Phys. B **17**, 2251 (1984).
12. E. Czuchaj, H. Stoll, H. Preuss, J. Phys. B **20**, 1487 (1987).
13. MOLPRO is a package of *ab initio* programs written by H.-J. Werner, P.J. Knowles with contributions from R.D. Amos, A. Berning, D.L. Cooper, M.J.O. Deegan, A.J. Dobbyn, F. Eckert, C. Hampel, G. Hetzer, T. Leininger, R. Lindh, A.W. Lloyd, W. Meyer, M.E. Mura, A. Nicklass, P. Palmieri, K. Peterson, R. Pitzer, P. Pulay, G. Rauhut, M. Schütz, H. Stoll, A.J. Stone, T. Thorsteinsson, H.-J. Werner, P.J. Knowles, J. Chem. Phys. **82**, 5053 (1985); P.J. Knowles, H.-J. Werner, Chem. Phys. Lett. **115**, 259 (1985); A. Berning, H.-J. Werner, P. Palmieri, P.J. Knowles, Mol. Phys. **98**, 1823 (2000).
14. E. Czuchaj, H. Stoll, Chem. Phys. **248**, 1 (1999).
15. E. Czuchaj, M. Krosnicki, H. Stoll, Theor. Chem. Acc. (in press).
16. D. Andrae, U. Häussermann, M. Dolg, H. Stoll, H. Preuss, Theor. Chim. Acta **77**, 123 (1990).
17. M. Dolg, H.-J. Flad, J. Phys. Chem. **100**, 6147 (1996).
18. A. Nicklass, M. Dolg, H. Stoll, H. Preuss, J. Chem. Phys. **102**, 8942 (1995).
19. W. Behmenburg, A. Makonnen, A. Kaiser, F. Rebentrost, V. Stämmler, M. Jungen, G. Peach, A. Devdariani, S. Tserkovnyi, A. Zagrebin, E. Czuchaj, J. Phys. B **29**, 3891 (1996).
20. J.E. Rice, P.R. Taylor, T.J. Lee, J. Almlöf, J. Chem. Phys. **94**, 4972 (1991).
21. D.E. Woon, T.H. Dunning Jr, J. Chem. Phys. **100**, 2975 (1994).
22. H.-J. Werner, Mol. Phys. **89**, 645 (1996).
23. S.F. Boys, F. Bernardi, Mol. Phys. **19**, 553 (1970).
24. M.S. Helmi, T. Grycuk, G.D. Roston, Chem. Phys. **209**, 53 (1996).
25. C. Bousquet, J. Phys. B **19**, 3859 (1986).
26. J. Koperski, M. Czajkowski, Eur. Phys. J. D **10**, 363 (2000).